teristics of inflammation, oedema, and vasodilatation. Experiments were also performed on age-matched control animals. Mice were anesthetized with ether or tribromoethanol (125 mg/kg). Intestinal segments from the middle third of the small intestine were extirpated and immediately stored in ice-cold phosphate-buffered saline. A segment (1 to 2 cm long) was opened along the antimesenteric border and pinned as a flat sheet (area 0.24 cm^2) between the two halves of an Ussing chamber, which contained a modified Krebs-Henseleit solution (5 ml; 114 mM NaCl, 25 mM $NaHCO_3$, 5 mM KCl, 1.65 mM NaH_2PO_4, 1.1 mM $MgCl_2$, 2.5 mM $CaCl_2$). The serosal bathing fluid contained glucose (10 mM), and the mucosal compartment mannitol (10 mM). The solutions were continuously bubbled with CO_2 (5%) in oxygen at 37°C. The transmural PD was monitored with a pair of calomel electrodes. Two types of Ussing chambers were used. In one type, the electrical field of the voltage clamp was perpendicular to the intestinal segment, which made it possible to estimate tissue resistance in absolute terms by using an automatic voltage clamp device to measure SCC. PD and SCC were recorded on a polygraph. Values of PD and SCC reported in the text, tables, and figures are given as the mean ± SEM. After mounting the tissue, the PD was allowed to stabilize for about 30 min. In control experiments, PD and SCC remained constant in infected and noninfected animals after this stabilizing period (*24*). For testing of drugs, each tissue was exposed to one drug in increasing concentrations with a 10-min interval between administrations. The drugs used were administered in volumes of 20 μl. At the end of the experiments, 200 μl of theophylline solution was added to the mucosal and serosal solutions to a final concentration of 1 mM to test tissue viability. If theophylline increased the PD by less than 40% of the control value, the experiment was discarded.

11. O. Lundgren *et al.*, data not shown.
12. The perfusion technique used was that described by Starkey *et al.* (*25*). Mice were anesthetized with tribromoethanol (125 mg/kg, i.p.). The abdomen was opened and a jejunal segment 4 to 6 cm long was chosen for the experiment. The intestinal segment was flushed with physiological saline and then placed in an organ bath containing a modified Krebs-Henseleit solution with glucose (122 mM NaCl, 25 mM $NaHCO_3$, 3.5 mM KCl, 1.2 mM KH_2PO_4, 1.2 mM $MgCl_2$, 2 mM $CaCl_2$, 30 mM glucose) continuously oxygenated with 5% CO_2 in oxygen at 37°C. The intestinal segment was perfused at a constant rate (990 μl $hour^{-1}$) through plastic tubes in both ends. The perfusion solution was identical to the solution in the organ bath except that glucose was substituted with mannitol. The perfusion solution also contained a radioactively labeled nonabsorbable marker (^{14}C-polyethylene glycol 4000; specific activity, 10 to 20 mCi g^{-1}; Amersham Pharmacia Biotech, Buckinghamshire, U.K.) at a concentration of ~0.07 μCi ml^{-1}. The tracer and plastic tubing were immersed in a solution containing nonlabeled polyethylene glycol 4000 (2 g ml^{-1}) for at least 24 hours before use. In control experiments this procedure prevented any adsorbance of the tracer to the plastic tubing. After placing the segment in the organ bath, the intestine was perfused for 20 min without sampling. Then 20-min samples were collected in tubes at the outflow end of the perfusion system. In one series of experiments (Fig. 2), in which the viability of the intestinal preparation was tested, the perfusion fluid was sampled during three consecutive 20-min periods. For reasons given in the text, only two samplings were performed in the experiments with drugs. Drugs were administered to the organ bath between the first and second sampling period. Radioactivity in duplicate samples was measured from the inflow and outflow solutions. The sample (100 μl) was mixed with 3.0 ml of scintillation fluid (Ultima Gold XR, Packard). At least 10,000 decays were measured in a Packard scintillation counter (Packard 1900 TR Liquid scintillation analyzer). Net fluid transport was estimated from the rate of perfusion, and the radioactivity of the solutions entering and leaving the intestine was determined (*26*). The transmural PD of the intestinal segment was recorded by two electrodes. One electrode was connected by a T-tube to the inlet of the perfusion system and the other was in contact with the solution in the organ bath. The PD was continuously recorded on a polygraph.
13. Diarrhea in the mice was judged by a scoring system, with a score of 1 indicating unusually loose yellow stool and a score of 4 a completely loose stool. A score of ≥2 (mucous with liquid stool, some loose but solid stool) was considered to indicate diarrhea. The scoring was performed by the same individual twice daily after administration of the rotavirus.
14. J. Cassuto, M. Jodal, O. Lundgren, *Acta Physiol. Scand.* **114**, 573 (1982).
15. J. R Mathias and M. H. Clench, in *Handbook of Physiology*, section 6, *The Gastrointestinal System*, vol. 1, *Motility and Circulation*, S. Schultz, Ed. (American Physiological Society, Bethesda, MD, 1989), pp. 1153–1178.
16. B. Hille, *Ionic Channels of Excitable Membranes* (Sinauer, Sunderland, MA, ed. 2, 1992).
17. I. Brunsson, A. Sjöqvist, M. Jodal, O. Lundgren, *Acta Physiol. Scand.* **130**, 633 (1987).
18. J. Cassuto, M. Jodal, R. Tuttle, O. Lundgren, *Scand. J. Gastroenterol.* **17**, 695 (1982).
19. K. Weclewicz, L. Svensson, K. Kristensson, *Brain Res. Bull.* **46**, 353 (1998).
20. A. Timar Peregrin, H. Ahlman, M. Jodal, O. Lundgren, *Acta Physiol. Scand.* **160**, 379 (1997).
21. A. Sjöqvist, J. Fahrenkrug, M. Jodal, O. Lundgren, *Acta Physiol. Scand.* **133**, 289 (1988); S. Eklund, A. Sjöqvist, J. Fahrenkrug, M. Jodal, O. Lundgren, *Acta Physiol. Scand.* **133**, 551 (1988).
22. F. Ruggeri, K. Johansen, G. Basile, J-P. Kraehenbuhl, L. Svensson, *J. Virol.* **72**, 2708 (1998).
23. L. Svensson, B. B. Finlay. D. Bass, C.-H. von Bonsdorff, H. B. Greenberg, *J. Virol.* **65**, 4190 (1991)
24. O. Lundgren *et al.*, unpublished observations.
25. W. G. Starkey *et al.*, *J. Pediatr Gastroenterol. Nutr.* **11**, 254 (1990).
26. H. Cooper, R. Levitan, J. S. Fordtran, F. J. Ingelfinger, *Gastroenterology* **50**, 1 (1966).
27. Supported by grants 28255 and 10392 from the Swedish Medical Research Council, and by the Knut and Alice Wallenberg Foundation.

10 June 1999; accepted 26 October 1999

A Role for Histone Acetylation in the Developmental Regulation of V(D)J Recombination

Michelle Taylor McMurry and Michael S. Krangel*

V(D)J recombination is developmentally regulated in vivo by enhancer-dependent changes in the accessibility of chromosomal recombination signal sequences to the recombinase, but the molecular nature of these changes is unknown. Here histone H3 acetylation was measured along versions of a transgenic V(D)J recombination reporter and the endogenous T cell receptor α/δ locus. Enhancer activity was shown to impart long-range, developmentally regulated changes in H3 acetylation, and H3 acetylation status was tightly linked to V(D)J recombination. H3 hyperacetylation is proposed as a molecular mechanism coupling enhancer activity to accessibility for V(D)J recombination.

V(D)J recombination is initiated by recombinase activating gene–1 (RAG-1)– and RAG-2–mediated cleavage between T cell receptor (TCR) and immunoglobulin coding gene segments (V, D, and J) and flanking recombination signal sequences (RSSs) (*1*). Chromosomal and nucleosomal RSSs are refractory to RAG-mediated cleavage relative to naked DNA (*2*, *3*), and V(D)J recombination is thought to be regulated in vivo by enhancer- and promoter-dependent changes in chromatin structure that provide RAG proteins access to specific RSSs (*4*). However, the nature of chromatin structural modifications associated with accessibility to RAG proteins is not known. Recent studies indicate that enhancers and promoters can direct the hyperacetylation of core histones (*5*) due to histone acetyltransferase activity of transcriptional coactivators (*6*). Moreover, histone hyperacetylation alters chromatin structure, as suggested by increased general sensitivity to endonucleases (*7*) and increased binding of transcription factors (*8*). Hyperacetylation of histones therefore provides a potential mechanism linking enhancer and promoter activity to RSS accessibility to RAG proteins.

We initially addressed the relation between histone acetylation and accessibility for V(D)J recombination by studying a TCRδ minilocus V(D)J recombination reporter in thymocytes of transgenic mice (Fig. 1, A and B). This reporter contains unrearranged human Vδ, Dδ, Jδ, and Cδ gene segments. With a functional enhancer in the Jδ3-Cδ intron, V, D, and J gene segments are all accessible to RAG proteins, and fully rearranged products (VDJ) are efficiently generated (*9*, *10*). With the enhancer deleted or mutated, only V-to-D rearrangement is observed (*9*, *11*, *12*). The failure of VD-to-J rearrangement without an enhancer reflects an inability of RAG proteins to access and cleave J segment RSSs (*13*). Because V and D accessi-

Department of Immunology, Post Office Box 3010, Duke University Medical Center, Durham NC 27710, USA.

*To whom correspondence should be addressed. E-mail: krang001@mc.duke.edu

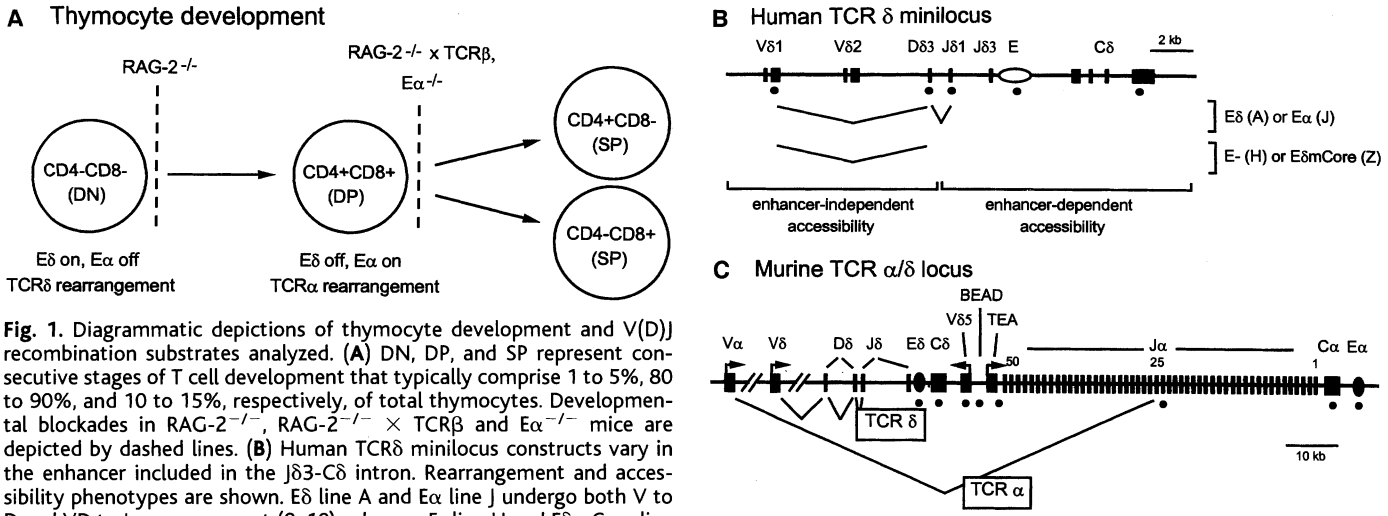

Fig. 1. Diagrammatic depictions of thymocyte development and V(D)J recombination substrates analyzed. (**A**) DN, DP, and SP represent consecutive stages of T cell development that typically comprise 1 to 5%, 80 to 90%, and 10 to 15%, respectively, of total thymocytes. Developmental blockades in RAG-2$^{-/-}$, RAG-2$^{-/-}$ × TCRβ and Eα$^{-/-}$ mice are depicted by dashed lines. (**B**) Human TCRδ minilocus constructs vary in the enhancer included in the Jδ3-Cδ intron. Rearrangement and accessibility phenotypes are shown. Eδ line A and Eα line J undergo both V to D and VD to J rearrangement (*9*, *10*), whereas E- line H and EδmCore line Z undergo only V to D rearrangement (*9*, *12*). Filled circles locate segments analyzed by CHIP. (**C**) Murine TCRα/δ locus. Typical TCRδ and TCRα rearrangement events (occurring in DN and DP thymocytes, respectively) are shown. Arrows identify transcriptional promoters. Filled circles locate segments analyzed by CHIP. BEAD, blocking element alpha delta; and TEA, T early alpha promoter and exon.

bility is maintained in an enhancer-independent manner, minilocus accessibility is sharply divided between an enhancer-independent 5′ region and an enhancer-dependent 3′ region.

To test whether accessibility reflects the acetylation status of minilocus chromatin, we measured histone H3 acetylation by a chromatin immunoprecipitation (CHIP) assay (*14*) using αAcH3 antiserum. Serially diluted DNA samples isolated from the input, αAcH3-bound, and -unbound fractions were tested by polymerase chain reaction (PCR) (Table 1) (*15*) to analyze specific sites along the minilocus. We initially compared a minilocus containing Eα [transgenic line J (*10*)] to one lacking an enhancer [transgenic line H (*9*)]. Eα turns on at the double positive (DP) stage and is therefore active in >95% of thymocytes (Fig. 1A) (*10*, *16*). Both Vδ1 and Cδ were hyperacetylated in unfractionated thymocytes of Eα line J, because they were heavily enriched in the αAcH3-bound fraction as compared with either the unbound fraction, the input fraction, or the bound fraction of a control immunoprecipitate (IP) (Fig. 2A). In contrast, the B cell–specific gene *Oct-2* was hypoacetylated, because it was poorly represented in the αAcH3-bound fraction and displayed a signal nearly equivalent to that in the bound fraction of the control. Acetylation at both Vδ1 and Cδ was sharply reduced in thymocytes of E- line H. Thus, Eα promotes H3 hyperacetylation at distant sites in the transgene. However, even without Eα, acetylation of Vδ1 was substantially above that of *Oct-2*. Thus, a component of Vδ1 acetylation is enhancer-independent.

To further analyze enhancer-dependent and -independent aspects of minilocus acetylation, we compared a minilocus containing a wild-type Eδ [transgenic line A (*9*)] to one in which Eδ is inactivated by a 3–base pair (bp) mutation in the binding site for CBF/PEBP2 [transgenic line Z (*12*)]. Because Eδ is only occupied and active in double negative (DN) thymocytes (*16*), both transgenes were bred onto the RAG-2$^{-/-}$ background (generating lines R×A and R×Z), in which thymocyte development is blocked at the DN stage (*17*). The lack of V(D)J recombination on this background also allowed analysis of a minilocus that was unrearranged in all thymocytes.

In DN thymocytes of Eδ line R×A, the minilocus was hyperacetylated along its entire length, with acetylation 25-fold over *Oct-2* for Vδ1; >100-fold over *Oct-2* for Dδ3, Jδ1, and Eδ; and 10-fold over *Oct-2* for Cδ (Fig. 2B) (*18*). This profile was markedly different in

Table 1. Primers and probes.

Gene segment	Oligonucleotide pairs for PCR from mononucleosomes		Probes or oligonucleotide pairs used to generate probes by PCR	
		Control		
Oct-2	Oct5:	5′-tggaggagctggaacagttt	Oct1:	5′-ttgcttagccccatccagg
	Oct6:	5′-tgtttggaccttggcatctttg	Oct6	
		Human TCRδ minilocus		
Vδ1	Vδ1-67:	5′-acaagttggtggtcatatta	Vδ1 (*20*)	
	Vδ1LU:	5′-cgatggcattctgttcatca		
Dδ3	Dδ3UI:	5′-agaagagccccaga	Dδ3 (*24*)	
	Dδ3H4:	5′-tatatggcccctgagaatcc		
Jδ1	Jδ1H1:	5′-gtgacaccgataaactc	Jδ1 (*20*)	
	Jδ1H3:	5′-ggaggatgccttaacctt		
Eδ	EδH3:	5′-cccttgaaagtcagccagag	EδH1:	5′-aaacaaggagatagggtgt
	EδH4:	5′-gctgaagccacttgataacag	EδH6:	5′-ctgctttcaacctgcttgag
Cδ	CδH3:	5′-ctctgctcaactgagcacta	Cδ (*20*)	
	CδH4:	5′-tcctccacgccatgcagaat		
		Endogenous murine TCRα/δ locus		
Cδ	MCD9:	5′-acttctcagtgcttcagac	MCD7:	5′-tatttacaggtgggctgac
	MCD12:	5′-cagggcttttgcttttcttc	MCD12	
Eδ	MED1:	5′-caaaatacatgcccagcca	MED1	
	MED2:	5′-cagcaaaactgataacccc	MED6:	5′-gggtttcttagaattatctgc
Vδ5	MVD9:	5′-ttcacagaaaatcgaccttga	MVD7:	5′-ggcacagtaataagtagcg
	MVD12:	5′-caatgcggattctccaaac	MVD12	
BEAD	MBD3:	5′-ttgcatacatgaggctctg	MBD1:	5′-ctgcttcactgaagagttc
	MBD6:	5′tgatgttccaaatatggcatg	MBD6	
TEA	TEA5:	5′-ctgtcccaagactttaagag	TEA1:	5′-tctttaccttcccagtgag
	TEA6:	5′-accaagacattctgttaccc	TEA6	
Jα25	MJA1:	5′-tgtgtgctagatcttgcc	MJA1	
	MJA2:	5′-gtgtcttggaatattgtgac	MJA6:	5′ggtgtatcttaaaattagccc
Cα	MCA5:	5′-tgggctgcagaacacaat	MCA1:	5′-taagtcctaagactggacc
	MCA6:	5′-tgttctttggctgtgtgag	MCA6	
Eα	MEA1:	5′-agatagtgaatcaatagccag	MEA1	
	MEA2:	5′-ttcaaaggggacctgttt	MEA6:	5′-gagagatcttatctctaactc

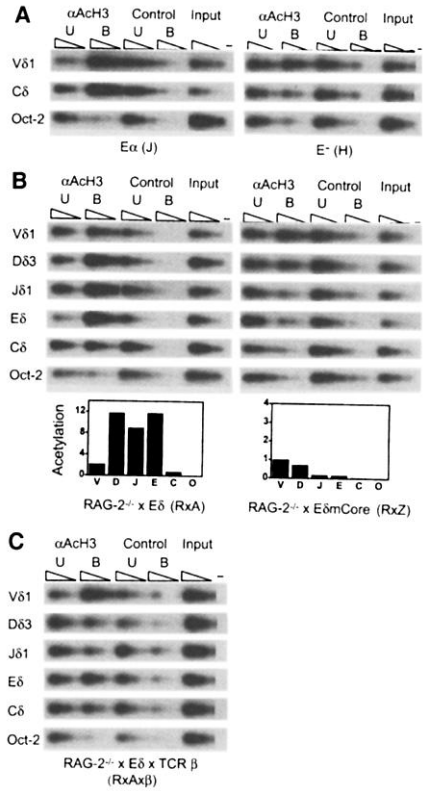

Fig. 2. H3 acetylation within a human TCRδ minilocus. (**A**) H3 acetylation was measured in total thymocytes of mice carrying minilocus constructs that include (J) or lack (H) Eα. CHIP was performed with anti-AcH3 or, as a control, no antibody, and serial threefold dilutions of bound (B), unbound (U), and input fractions were analyzed by PCR. (**B**) H3 acetylation was measured as in (A) in the DN thymocytes of RAG-$2^{-/-}$ mice carrying a minilocus with either a wild-type (R×A) or a mutant (R×Z) Eδ. Acetylation is plotted as B/U, calculated as described (*18*). (**C**) H3 acetylation was measured as in (A) in the DP thymocytes of RAG-$2^{-/-}$ × TCRβ transgenic mice carrying a minilocus with a wild-type Eδ (R×A×β). Control CHIP was with normal rabbit serum.

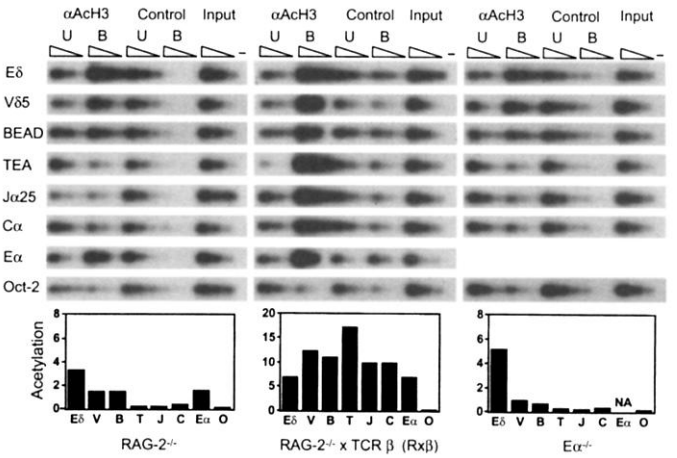

Fig. 3. H3 acetylation within the endogenous murine TCRα/δ locus. H3 acetylation measured in the DN thymocytes of RAG-$2^{-/-}$ mice (*27*), the DP thymocytes of RAG-$2^{-/-}$ × TCRβ (R×β) mice, and the DP thymocytes of Eα$^{-/-}$ mice. Control CHIP was with normal rabbit serum. Acetylation is plotted as in Fig. 2B. NA, not applicable.

thymocytes of EδmCore line R×Z. Acetylation at Vδ1 and Dδ3 was 25- and 18-fold, respectively, over *Oct-2*. However, acetylation at Jδ1, Eδ, and Cδ was much lower. Thus, the histone H3 acetylation patterns of the Eδ and EδmCore miniloci are fully consistent with the previously determined patterns of V(D)J recombination and accessibility to RAG proteins. Concordance of the acetylation and accessibility profiles leads us to propose that enhancer-independent acetylation of V and D gene segments allows for enhancer-independent minilocus V-to-D rearrangement, whereas enhancer-dependent acetylation of J gene segments allows for enhancer-dependent minilocus VD-to-J rearrangement.

Eδ is inactivated upon transit of thymocytes from DN to DP due to loss of occupancy at binding sites for CBF/PEBP2 and c-Myb (*16*). To investigate changes in histone H3 acetylation across this developmental transition, we bred a rearranged TCRβ transgene into Eδ line R×A to generate R×A×β mice, in which nearly 100% of thymocytes are DP (*19*). Enhancer-dependent acetylation was largely extinguished across the transgene, with the exception of some residual acetylation over Eδ itself (Fig. 2C). Thus, developmental loss of Eδ occupancy causes a marked reduction in minilocus H3 acetylation. Enhancer-independent acetylation at Vδ1 was maintained in DP thymocytes, but that at Dδ3 was extinguished. Enhancer-independent acetylation of these elements appears to be under distinct control.

To further probe the relation between H3 acetylation and accessibility for V(D)J recombination, we measured developmental changes in acetylation at the endogenous TCRα/δ locus (Fig. 1C). This locus contains distinct sets of gene segments that are activated for V(D)J recombination at different stages of T cell development (*20*). TCRδ rearrangement (Vδ-Dδ-Jδ) occurs in DN thymocytes and TCRα rearrangement (Vα-Jα) in DP thymocytes (Fig. 1A). Eδ activity at the DN stage (*10*, *16*) is partly responsible for TCRδ accessibility, because TCRδ rearrangement is partially inhibited in Eδ$^{-/-}$ mice (*21*). TCRα rearrangement is markedly impaired in Eα$^{-/-}$ mice (*22*), indicating that Eα activity at the DP stage (*10*, *16*) is critical for accessibility across the 70-kb Jα region. Eα is also required for transcription from the germ line T early alpha (TEA) promoter 5′ of Jα segments, and up-regulates TCRδ transcription as well (*22*).

We analyzed RAG-$2^{-/-}$ mice (*17*) to assess acetylation in DN thymocytes, RAG$2^{-/-}$ × TCRβ (R×β) mice (*19*) to assess acetylation in DP thymocytes, and Eα$^{-/-}$ mice [which, like R×β mice, are blocked at DP (*22*)] to assess the effect of Eα. The DN compartment (RAG-$2^{-/-}$) is characterized by a hyperacetylated TCRδ region [Eδ, Cδ (*23*), and Vδ5] and a hypoacetylated TCRα region (TEA, Jα25, and Cα) (Fig. 3). The blocking element alpha delta (BEAD) region spanning Vδ5 to TEA, previously shown to have enhancer-blocking activity (*24*), appears to be a transition zone. Notably, although the Jα-Cα region is hypoacetylated in DN thymocytes, Eα itself is hyperacetylated. Because Eα is occupied but inactive in DN thymocytes (*16*), local acetylation over Eα likely relates to its occupancy, rather than activity.

The transition to DP (R×β) was marked by a pronounced shift to a hyperacetylated state over the entire Jα-Cα region, and an increase in acetylation over Vδ5 (Fig. 3) and Cδ (*23*). These changes reflect activation of Eα, because they were not detected in DP thymocytes of Eα$^{-/-}$ mice. Thus, Eα modulates histone acetylation over at least 85 kb, paralleling its effects on both V(D)J recombination and transcription. Although Eδ itself is inactivated on transition to DP (*16*), H3 acetylation in the TCRδ region was maintained in Eα$^{-/-}$ DP thymocytes. Thus, TCRδ acetylation is determined, at least in part, by elements other than Eδ, a notion consistent with the residual TCRδ rearrangement in Eδ$^{-/-}$ mice (*21*).

In summary, analysis of both a transgenic V(D)J recombination reporter substrate and the endogenous TCRα/δ locus indicate Eδ and Eα to be long-range developmental regulators of H3 acetylation. H3 hyperacetylation is a consequence of enhancer occupancy, because a 3-bp Eδ mutation that prevents CBF/PEBP2 binding prevents enhancer-dependent minilocus H3 hyperacetylation. Nevertheless, the precise mechanism that translates enhancer occupancy into long-range changes in histone acetylation is not known. In both the minilocus and the endogenous locus, regions displaying H3 hyperacetylation were invariably those displaying accessibility to the recombinase. Because H3 hyperacetylation is highly predictive of gene segment accessibility yet exists in the absence of recombination (i.e., on a Rag-$2^{-/-}$ background), we propose that it plays a primary role in establishing accessibility for V(D)J recombination. Histone hyperacetylation was recently reported not to affect accessibility of mononucleosomal RSSs to recombinant RAG proteins in a simple

in vitro system (*3*). Acetylation-dependent accessibility may therefore require more-complex chromosomal substrates or remodeling activities that are present in vivo but not yet reproduced in vitro. We suggest a model for V(D)J recombination in which cis-regulatory elements direct access to RAG proteins in vivo by inducing the region- and developmental stage–specific hyperacetylation of histone H3.

References and Notes

1. M. Gellert, *Adv. Immunol.* **64**, 39 (1997); D. G. Schatz, *Sem. Immunol.* **9**, 149 (1997); U. Grawunder, R. B. West, M. R. Lieber, *Curr. Opin. Immunol.* **10**, 172 (1998).
2. P. Stanhope-Baker, K. M. Hudson, A. L. Shaffer, A. Constantinescu, M. S. Schlissel, *Cell* **85**, 887 (1996); J. Kwon, A. N. Imbalzano, A. Matthews, M. A. Oettinger, *Mol. Cell* **2**, 829 (1998).
3. A. Golding, S. Chandler, E. Ballestar, A. P. Wolffe, M. S. Schlissel, *EMBO J.* **18**, 3712 (1999).
4. B. P. Sleckman, J. R. Gorman, F. W. Alt, *Annu. Rev. Immunol.* **14**, 459 (1996); M. S. Schlissel and P. Stanhope-Baker, *Sem. Immunol.* **9**, 161 (1997); W. M. Hempel, I. Leduc, N. Mathieu, R. K. Tripathi, P. Ferrier, *Adv. Immunol.* **69**, 309 (1998).
5. P. L. Sheridan, T. P. Mayall, E. Verdin, K. A. Jones, *Genes Dev.* **11**, 3327 (1998); L. Madisen, A. Krumm, T. R. Hebbes, M. Groudine, *Mol. Cell. Biol.* **18**, 6281 (1998); M.-H. Kuo, J. Zhou, P. Jambeck, M. E. A. Churchill, C. D. Allis, *Genes Dev.* **12**, 627 (1998); B. S. Parekh and T. Maniatis, *Mol. Cell* **3**, 125 (1999).
6. A. P. Wolffe, J. Wong, D. Pruss, *Genes Cells* **2**, 291 (1997); K. Struhl, *Genes Dev.* **12**, 599 (1998); J. L. Workman and R. E. Kingston, *Annu. Rev. Biochem.* **67**, 545 (1998).
7. T. R. Hebbes, A. L. Clayton, A. W. Thorne, C. Crane-Robinson, *EMBO J.* **13**, 1823 (1994).
8. D. Lee, J. J. Hayes, D. Pruss, A. P. Wolffe, *Cell* **72**, 73 (1993); M. Vettese-Dadey *et al.*, *EMBO J.* **15**, 2508 (1996).
9. P. Lauzurica and M. S. Krangel, *J. Exp. Med.* **179**, 43 (1994).
10. ———, *J. Exp. Med.* **179**, 1913 (1994).
11. C. Hernandez-Munain, P. Lauzurica, M. S. Krangel, *J. Exp. Med.* **183**, 289 (1996).
12. P. Lauzurica, X.-P. Zhong, M. S. Krangel, J. L. Roberts, *J. Exp. Med.* **185**, 1193 (1997).
13. M. T. McMurry, C. Hernandez-Munain, P. Lauzurica, M. S. Krangel, *Mol. Cell. Biol.* **17**, 4553 (1997).
14. Mononucleosomes were prepared from thymocytes of 4- to 8-week-old mice with modifications from Hebbes *et al.* (*7*). Thymocytes (1×10^9 to 4×10^9) were filtered through nylon mesh, centrifuged (350*g*, 7 min), and the pellet resuspended at 4×10^7 cells/ml in 0.15 M NH_4Cl, 1 mM $KHCO_3$, 0.1 mM Na_2EDTA, 10 mM sodium butyrate, 0.1 mM phenylmethylsulfonyl fluoride (PMSF), and 0.1 mM benzamidine (pH 7.4) for 5 min at 23°C to lyse red blood cells. Thymocytes were then washed twice and resuspended at 1×10^8/ml in lysis buffer [80 mM NaCl, 10 mM tris-HCl (pH 7.5), 10 mM sodium butyrate, 6 mM $MgCl_2$, 1 mM $CaCl_2$, 250 mM sucrose, 0.1 mM PMSF, and 0.1 mM benzamidine], and an equal volume of buffer containing 0.04% (v/v) NP-40 was added for 5 min at 4°C. Nuclei were pelleted through 30% sucrose by centrifugation at 350*g* for 7 to 14 min and washed once, and were then resuspended in digestion buffer at 5 mg/ml (7×10^8 nuclei/ml) by absorbance at 260 nm. Nuclei were incubated with 1000 U/ml micrococcal nuclease (Worthington, Freehold, NJ) for 10 min at 37°C to produce a partial digest (*25*). After shift to 0°C and addition of Na_3EDTA to 5 mM, the digest was centrifuged at 13,000*g* for 1 min at 4°C, the pellet was washed, and supernatants from the two centrifugations were combined and NaCl added to 50 mM. Histone H1 was removed by incubation for 1.5 hours at 4°C with 30 mg/ml Sephadex CM-25, followed by centrifugation for 5 min at 13,000*g*. A Biocomp Gradient Mate (Accurate Chemical and Scientific, Westbury, NY) was used to prepare 14 ml of 10 to 45% linear sucrose gradients in 10 mM tris-HCl (pH 7.5), 0.25 mM Na_3EDTA (pH7.0), 10 mM sodium butyrate, 100 mM NaCl, 0.1 mM PMSF, and 0.1 mM benzamidine, and 2 to 3 mg of H1-depleted, digested chromatin was loaded onto each gradient and centrifuged for 18 hours at 40,000 rpm in an SW-40 rotor (Beckman Instruments, Fullerton, CA) at 4°C. Mononucleosome-containing fractions were identified as described (*26*). Immunoprecipitation of freshly prepared mononucleosomes (25 to 40 μg) was performed as described (*7*), with modifications. Pooled gradient fractions were first treated with 0.6 μl of 50% salmon sperm DNA–protein A-Sepharose slurry per μg of mononucleosomes for 30 min at 4°C, followed by centrifugation for 5 min at 13,000*g*. The supernatant was incubated with antibody to diacetylated histone H3–purified rabbit immunoglobulin G (IgG) (Upstate Biotechnology, Lake Placid NY) or control rabbit IgG (Sigma) (0.25 μg/μg of DNA) for 16 hours, followed by addition of salmon sperm DNA–protein A-Sepharose (12 μl/μg of antibody) for 1 hour. After centrifugation, the supernatant was retained, the IP washed, and DNA purified from these and input fractions (*7*).
15. Serial threefold dilutions (60, 20, and 6.6 ng) of bound, unbound, and input DNA fractions were analyzed by 25 cycles of PCR (45 s at 94°C, 1 min at 55°C or 59°C, and 2 min at 72°C) in 25-μl reactions as described (*13*). A single serial dilution series produced from each DNA fraction was typically used for PCR reactions with all primer sets. Primers and probes are listed in Table 1. Primer pairs were screened initially for their ability to amplify pure mononucleosomal DNA as efficiently as unfractionated genomic DNA. PCR products (which ranged in size from 99 to 150 bp) were subjected to electrophoresis through 3% Nusieve 3:1 agarose gels (FMC Bioproducts, Rockland, ME) and transferred to Magna Charge nylon membranes (0.22 μm; Osmonics, Westborough, MA). Probes were ^{32}P-labeled by random priming.
16. C. Hernandez-Munain, B. P. Sleckman, M. S. Krangel, *Immunity* **10**, 723 (1999).
17. Y. Shinkai *et al.*, *Cell* **68**, 855 (1992).
18. Acetylation was quantified by PhophorImager (Molecular Dynamics) analysis of Southern blots. Values of B/U are reported, where B is the bound fraction of the αAcH3 IP and U is the unbound fraction of the control IP. The latter was used instead of the unbound fraction of the αAcH3 IP to prevent the ratios from being artificially inflated by depletion of the unbound fraction in instances of heavy acetylation. B/U ratios were calculated by determining the displacement between the B and U titration curves.
19. Y. Shinkai *et al.*, *Science* **259**, 822 (1993).
20. M. S. Krangel *et al.*, *Immunol. Rev.* **165**, 131 (1998).
21. R. J. Monroe *et al.*, *Immunity* **10**, 503 (1999).
22. B. P. Sleckman, C. G. Bardon, R. Ferrini, L. Davidson, F. W. Alt, *Immunity* **7**, 505 (1997).
23. M. T. McMurry and M. S. Krangel, unpublished observations.
24. X.-P. Zhong and M. S. Krangel, *Proc. Natl. Acad. Sci. U.S.A.* **94**, 5219 (1997).
25. Southern blot analysis of titrated nuclease digests indicated that the sensitivity to nuclease digestion of analyzed sequences was similar to that of bulk DNA.
26. J. J. Hayes and K.-M. Lee, *Methods* **12**, 2 (1997).
27. The RAG-$2^{-/-}$ sample is actually R×A, but is designated RAG-$2^{-/-}$ for clarity because the endogenous locus rather than the transgene is analyzed. The *Oct-2* panel for this sample is identical to that for R×A in Fig. 2B.

28. We thank B. Sleckman, Y. Zhuang, and C. Doyle for comments on the manuscript and encouragement, and C. Hernandez-Munain for advice. Supported by NIH grant GM 41052. M.T.M. was supported in part by an NIH Medical Scientist Training Grant and a United Negro College Fund–Merck Graduate Science Research Dissertation Fellowship.

16 September 1999; accepted 24 November 1999

A Critical Role for Murine Complement Regulator Crry in Fetomaternal Tolerance

Chenguang Xu,[1]* Dailing Mao,[1]* V. Michael Holers,[2] Ben Palanca,[1] Alec M. Cheng,[1] Hector Molina[1,3]†

Complement is a component of natural immunity. Its regulation is needed to protect tissues from inflammation, but mice with a disrupted gene for the complement regulator decay accelerating factor were normal. Mice that were deficient in another murine complement regulator, Crry, were generated to investigate its role in vivo. Survival of *Crry*$^{-/-}$ embryos was compromised because of complement deposition and concomitant placenta inflammation. Complement activation at the fetomaternal interface caused the fetal loss because breeding to *C3*$^{-/-}$ mice rescued *Crry*$^{-/-}$ mice from lethality. Thus, the regulation of complement is critical in fetal control of maternal processes that mediate tissue damage.

Activation of complement promotes natural immunity by inducing chemotaxis of inflammatory cells, enhancing phagocytosis by neutrophils and monocytes, facilitating immune complex clearance, and mediating cell lysis by the membrane attack complex (*1*). Complement can also bind and attack self tissues, especially in areas of active inflammation. In vitro studies have shown that cells are protected from the deleterious effects of complement by proteins that regulate complement activation (*2*).

Three membrane-bound proteins regulate the activation of the third and fourth components of complement (C3 and C4) on the

[1]Departments of Medicine and Pathology, Washington University School of Medicine, St. Louis, MO 63110, USA. [2]Departments of Medicine and Immunology, University of Colorado Health Science Center, Denver, CO 80262, USA. [3]Veteran's Administration Medical Center, St. Louis, MO 63106, USA.

*These authors contributed equally to this work.
†To whom correspondence should be addressed. E-mail: hmolina@imgate.wustl.edu